

Process Modeling in Laser Deposition of Multilayer SS410 Steel

Liang Wang

Center for Advanced Vehicular Systems,
Mississippi State University,
Mississippi State, MS 39762
e-mail: liangw@cavs.msstate.edu

Sergio Felicelli

Mechanical Engineering Department,
Mississippi State University,
Mississippi State, MS 39762
e-mail: felicelli@me.msstate.edu

A three-dimensional finite element model was developed to predict the temperature distribution and phase transformation in deposited stainless steel 410 (SS410) during the Laser Engineered Net Shaping (LENS™) rapid fabrication process. The development of the model was carried out using the SYSWELD software package. The model calculates the evolution of temperature in the part during the fabrication of a SS410 plate. The metallurgical transformations are taken into account using the temperature-dependent material properties and the continuous cooling transformation diagram. The ferritic and martensitic transformation as well as austenitization and tempering of martensite are considered. The influence of processing parameters such as laser power and traverse speed on the phase transformation and the consequent hardness are analyzed. The potential presence of porosity due to lack of fusion is also discussed. The results show that the temperature distribution, the microstructure, and hardness in the final part depend significantly on the processing parameters. [DOI: 10.1115/1.2738962]

Keywords: laser deposition, phase transformation, porosity, hardness

Introduction

The Laser Engineering Net Shaping (LENS™) process is a laser-assisted, direct metal manufacturing process for rapid fabrication [1–3]. Figure 1 shows the schematic of the LENS fabrication process. The LENS fabricated part is built on a solid substrate usually made of the metal to be deposited or similar material. Initially, the laser beam is focused on the substrate to create a molten pool, where metallic powder particles are simultaneously injected by a set of converging nozzles. A single layer of material is built up when the substrate moves beneath the laser beam in the x - y plane under computer guidance. After deposition of a single layer, the laser beam and the powder delivery nozzle assembly is incremented in the positive z direction to begin the deposition of subsequent layers. Accordingly, the process is repeated and a three-dimensional part is built up in a layer-by-layer manner.

The feasibility of depositing different metals including stainless steel, tool steel, nickel-based superalloys, and titanium into near-net shape parts in a single processing step has been illustrated using LENS rapid fabrication technology in the past [4–6]. However, the nonuniform microstructure and properties found in the parts built by LENS may restrain the wide acceptance of this process in industry [6]. In order to fully understand the microstructure and properties of LENS-deposited materials, it is essential to investigate the effects of processing parameters on the thermal history at each point of the part, as well as the solid-state phase transformations that may occur during the process. Numerical simulation methods have the potential to provide such knowledge based on a suitable physical computational model. Numerical models have been undertaken by several authors to simulate the thermal behavior [1–8] and microstructure evolution [9–15] during the laser deposition process. The results of these models can provide insight into how processing parameters can be manipulated to obtain favorable metallurgical structures and mechanical properties.

When a layer of material is being deposited, several previously

deposited layers can be reheated or remelted, which under unfavorable process conditions may lead to undesired effects. For example, during the LENS deposition of steel, martensite can be reheated above the martensite start temperature, leading to tempered martensite after posterior cool-down. However, if the process parameters are controlled such that most of the part remains at temperatures higher than the martensite start temperature, after cool-down this will lead to a uniform microstructure consisting of nontempered martensite with minor proportions of retained austenite and carbides. The resulting hardness is also high and uniformly distributed [9–11]. Costa et al. [12–14] investigated the effects of the substrate size and the idle time between the deposition of consecutive layers of material on the phase transformation and hardness distribution in SS420 parts built by a laser powder deposition process similar to LENS. They found that short idle time and small substrate size can reduce the proportion of tempered martensite and lead to a more uniform microstructure and property distribution. This is because both short idle time and small substrate size are more likely to keep most of the part at temperatures higher than the martensite start temperature.

The size of the molten pool is a suitable monitor to optimize the processing parameters during the LENS process. The temperature distribution and cooling rate at the solid-liquid interface of the molten pool affect the microstructural features, which determine the strength and ductility of the deposited part [5]. The effects of the laser-processing parameters (laser power and scanning speed) on the molten pool size have been investigated both by experiments [16] and modeling [17,18]. There are several works that have investigated the transport phenomena in and around the molten pool, including solidification, microstructure formation, and effects of powder injection and pulsing lasers [19–21]; however, these works were done in the context of the laser cladding process and do not focus on the issues presented in this paper which refer to phenomena observed during the building of a part with the LENS process.

In this model, a heat transfer calculation is coupled with solid phase transformation kinetics data on the ferritic and martensitic transformation and austenitization using the SYSWELD software package [22–24]. By calculating the phase transformations in a SS410 plate during the LENS deposition, the model can infer consequent changes in the hardness of the deposited part. The

Contributed by the Manufacturing Engineering Division of ASME for publication in the JOURNAL OF MANUFACTURING SCIENCE AND ENGINEERING. Manuscript received October 27, 2006; final manuscript received March 13, 2007. Review conducted by Y. Lawrence Yao.

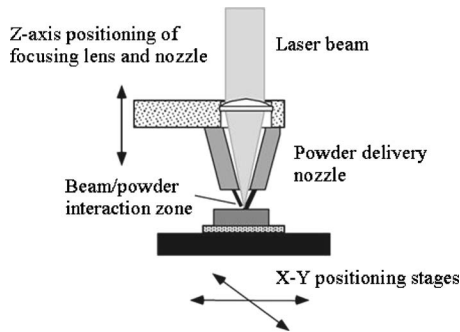


Fig. 1 Schematic of LENS process

laser power is adjusted and optimized in order to produce a pre-defined steady molten pool size for different laser traverse speeds. The effects of laser power and traverse speed on the thermal history, phase proportions, and consequent hardness of the processed material during the LENS deposition of a ten-layer wall of SS410 are studied. The potential presence of porosity due to the lack of fusion in certain regions of the part is also discussed.

Mathematical Model

A three-dimensional finite element model was developed to simulate the LENS process using the commercial code SYSWELD. The model was used to predict the temperature distribution and solid-phase transformation of a thin-walled structure (plate) of AISI 410 stainless steel (SS410).

Heat Transfer Analysis. In the heat transfer calculations, the heat conduction equation was solved numerically using the finite element method. The density, thermal conductivity, and specific heat are dependent on temperature and material phase. In addition to the solid phase transformations, the latent heat of the solid-liquid phase change is also considered through the enthalpy function. It was assumed that the substrate material is initially at room temperature, T_0 (no preheating). A fixed temperature boundary condition equal to the room temperature is prescribed on the bottom surface of the substrate. The boundary conditions for all other surfaces take into account both laser heating and heat losses due to surface convection and radiation. Nd:YAG laser is used in the calculation. The laser beam power is modeled as a Gaussian profile with a conical shape, described by [25]:

$$Q_r = \frac{2P}{\pi r_0^2 H} \left(1 - \frac{z}{H}\right) \exp\left(1 - \left(\frac{r}{r_0}\right)^2\right) \quad (1)$$

where Q_r is the input energy density (W/mm^3), P the absorbed laser beam power (W), r_0 the initial radius (at the top of the keyhole) ($=0.5$ mm), then the laser beam size is equal to 1.0 mm, H the depth ($=0.5$ mm), r the current radius, i.e., the distance from the cone axis, and z is the current depth. The moving heat source was modeled by a user subroutine in SYSWELD.

During the LENS process, part of the energy generated by the laser beam is lost before being absorbed by the deposited material. Measurements done in Ref. [26] revealed that the laser energy transfer efficiency was in the range of 30–50%. This indicates that more than half of the incident laser energy is never transferred to the deposited material. There are many factors that can affect laser beam absorption. One of the main reasons is the laser beam irradiance on the fabricated part. Furthermore, other complex phenomena occur in the molten pool, such as solute partitioning, evaporation and marangoni convection, which are not taken into account in the current study. In this work, the nominal laser power is calibrated by matching the thermal profile surrounding the molten pool with the experimental data of Ref. [3]. The details and results of this calibration are reported in Ref. [18].

The model uses a fixed mesh for the plate and substrate, where

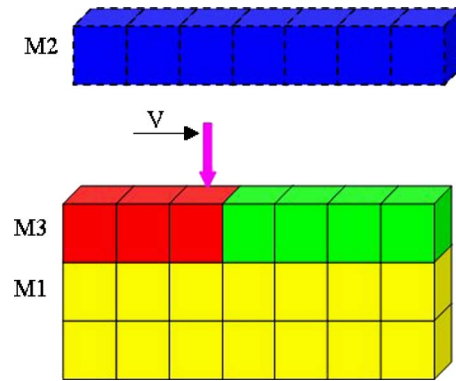


Fig. 2 Sketch to illustrate dummy material method for the element activation. M1: deposited layers and substrate, material with actual thermal properties and phase transformation; M2: layers to be deposited, material with dummy low thermal properties and without phase transformation; M3: layer being deposited, material with actual thermal properties and dummy phase.

the mesh elements of the plate are initially inactive and are activated during material deposition. Two different approaches are available to model material deposition in SYSWELD. One is activation/deactivation of elements, which uses a formulation to activate and deactivate individual elements; another is the dummy material method, in which the elements are activated layer by layer. In the current study, a dummy material method that uses three different types of material is employed for the element activation. A graphical representation of the different material types is shown in Fig. 2.

The first material, M1, is used for the substrate and the elements of layers that have already been deposited; this material is assigned the actual thermal and metallurgical properties of SS410. The initial phase of the substrate is assumed to be ferrite. Austenitization may occur when the temperature exceeds the austenitization temperature. The martensitic and ferritic transformations may occur during cooling in the substrate and in the layers that have been deposited, depending on the cooling rate and temperature. The second material, M2, is used for elements of layers that have not yet been deposited. These elements are assigned dummy low values of the thermal properties, which means that the material cannot be heated up, and therefore cannot transform to austenite. No metallurgical properties (phase transformations) are required for the second material. A third type of material, M3, is used for the elements that are being deposited. These elements are initially in the dummy phase but they are assigned the actual thermal properties of SS410 so that they can heat up. Once they reach the austenitization temperature, the dummy phase is switched to austenite and the actual metallurgical behavior (subsequent transformation to martensite or ferrite) is modeled after that.

Phase Transformation and Hardness Model. Based on the thermal cycles at each point, the phase transformations that may occur in the material are predicted using semi-empirical models. The hardness of the material was assumed to be equal to the weighted average of the hardnesses of individual phases when the part cools down to room temperature. It assumes that three possible phases could be present in the part when the part is finished, including retained austenite, fresh martensite, and tempered martensite. Therefore, the hardness can be calculated by

$$H = f_\gamma H_\gamma + f_{M0} H_{M0} + (1 - f_\gamma - f_{M0}) H_M \quad (2)$$

where H_γ , H_{M0} , and H_M are the hardness of austenite, fresh martensite, and tempered martensite, respectively; f_γ and f_{M0} are the volume fraction of austenite and fresh martensite, respectively. The hardness of austenite and fresh martensite was assumed to be

260 and 660 HV, respectively [12]. The hardness of tempered martensite takes into account the anisothermal tempering process via [12]:

$$H_M = H_{M0} - A \left\{ \int_{t_1}^{t_2} \exp\left(-\frac{Q}{RT(t)}\right) dt \right\}^m \quad (3)$$

where Q is the activation energy, R the universal gas constant (equal to 8.314 J/m K), and A and m fitting constants. Based on the data published by Costa et al. [12], $Q=250$ kJ/mol, $A=1300$ HV/s, and $m=0.055$.

The proportion of retained austenite for each thermal cycle is given by

$$f_{\gamma i} = f_{\gamma 0} \exp\left(-\frac{(M_S - T_i)}{90.9}\right) \quad \text{for } T_i \leq M_S \quad (4)$$

where $f_{\gamma 0}$ and $f_{\gamma i}$ are the volume fractions of retained austenite before and after thermal cycle i in which the part cools down to the temperature T_i .

If the part is reheated up to or above the austenization temperature A_{c3} ($=1015^\circ\text{C}$), the martensite will transform to austenite completely. In order to calculate the final phase proportion, including tempered martensite, the calculation should start at the first thermal cycle in which the maximum temperature is lower than A_{c3} .

If there are n thermal cycles, the proportion of retained austenite when the part cools down to room temperature is given by

$$f_{\gamma} = f_{\gamma 0} \eta_1 \eta_2 \eta_3 \cdots \eta_n \quad (5)$$

where η_i is given by

$$\eta_i = \exp\left(-\frac{(M_S - T_i)}{90.9}\right) \quad (i = 1, 2, \dots, n) \quad (6)$$

The proportion of fresh martensite when the part cools down to room temperature is equal to the proportion of martensite transformed from austenite in the final thermal cycle.

Model Application

The model described in the previous section was calibrated with the experiments of Hofmeister et al. [3] in order to capture the effective laser power transferred to the material. The procedure, described in Ref. [18], showed a good agreement between the calculated results and experimental data for the temperature profile and cooling rate on the top surface of the part. It is noted that SS316 was used in the experiments of Hofmeister et al., however, the experimental results are considered effective for this model since the thermal properties of SS316 are very similar to those of SS410. In the present work, the thermally calibrated model was used to study the influence of the laser power and traverse speed on the final phase proportion and properties of a ten layer thin-walled plate of AISI 410 stainless steel, deposited by the LENS process. The geometry and finite element mesh used in the model are shown in Fig. 3.

The structure was built by overlapping ten single tracks of material, each with a length of 10.0 mm, a thickness of 0.5 mm, and a width of 1.0 mm. The plate was fabricated on the surface of a substrate 5 mm thick, 10 mm wide, and 20 mm long. The number of nodes in the mesh is 104,535, and the number of elements is 132,400. The element size in the part is $0.1 \times 0.1 \times 0.1$ mm³. The chemical composition of SS410 is given in Table 1. The density, thermal conductivity, and specific heat are dependent on temperature and material phase, as shown in Fig. 4.

Three cases are studied, as shown in Table 2, in which the traverse speed of the laser beam is 2.5, 7.62, and 20 mm/s, respectively. The idle time between depositions of consecutive layers for each case is 1.0, 0.7, and 0.5 s, respectively. The laser beam moves in the same direction (left to right) for each pass.

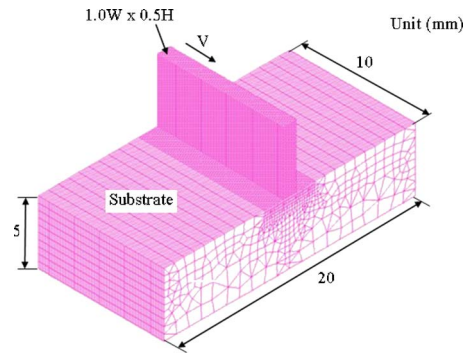


Fig. 3 Geometry and mesh to simulate the LENS process for a ten layer plate

Results and Discussions

The laser power is adjusted in order to achieve a steady molten pool size and temperature distribution surrounding the molten pool during the LENS process. Figure 5(a) shows the nominal laser power used for each pass at different traverse speeds. Higher laser power is required for higher traverse speed. A steady linear decrease of $\sim 5\%$ of the laser power is reached after deposition of the fifth layer. At the beginning of each pass, a higher laser power is applied in order to fully melt the powder, while a lower laser power is used near the end of each pass. The change of laser power for each pass is achieved by the laser power intensity, as shown in Fig. 5(b). The actual laser power is equal to the product of the nominal laser power and the laser power intensity.

In order to achieve a fully dense material, one or more previous layers should be melted as a new layer is deposited in order to maintain a continuous molten pool from layer to layer. The number of melted layers depends on the laser power and traverse speed chosen. Figure 6 shows the molten pool size and shape when the laser beam moves to the center of the part at the tenth layer for each laser traverse speed. The molten pool size is determined by the melting temperature of SS410 (1450°C). About one and a half layers are melted for each pass. It is observed that for the highest traverse speed (Fig. 6(c)), the shape of the molten pool has become elongated and it hardly penetrates into the second layer.

Figure 7 shows the thermal cycles at the midpoints of deposited layers 1, 3, 5, and 10 at the laser traverse speed of 2.5 mm/s. Each peak indicates that the laser beam passes over or near the pre-defined location, from initial layer to subsequent layer depositions. At the midpoint of the first layer, the initial peak in temperature is approximately 2060°C . After that, the heat is quickly conducted away to around 100°C at $t=5$ s for the first layer. This indicates that the idle time between the depositions of the first two consecutive layers is enough to cool down the deposited part. The solidification process in the initial thermal cycle during the first pass should result in a high strength, martensitic microstructure with minimal retained ferrite due to the high cooling rate. However, each subsequent pass reheats the previous layers to above the martensite starting temperature ($M_S=350^\circ\text{C}$ for SS410 [27]), which results in the tempered martensite transformation. After the fifth layer is deposited, the first layer still receives a thermal hit of 650°C . After each deposition pass, the part cools down, but the

Table 1 Chemical composition of SS410 steel (wt %)

C	Si	Mn	Cr	P	S
0.12/0.17	<1.0	<1.0	12.0/14.0	<0.04	<0.03

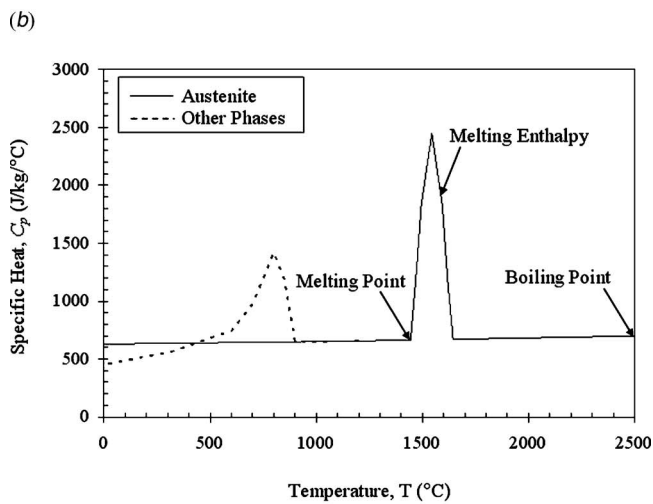
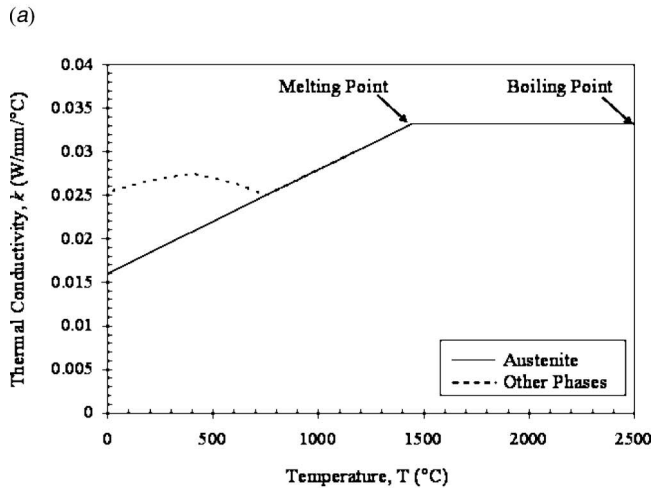
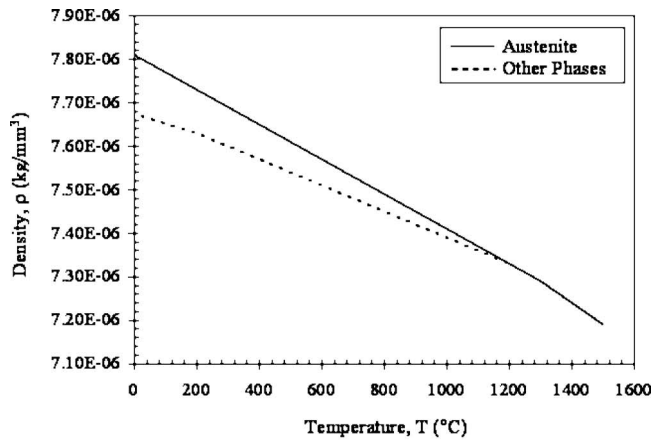


Fig. 4 Thermal properties used for SS410, (a) density, (b) thermal conductivity, and (c) specific heat

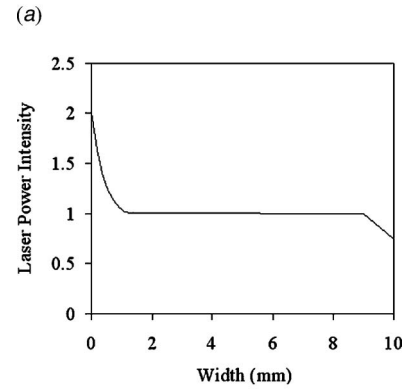
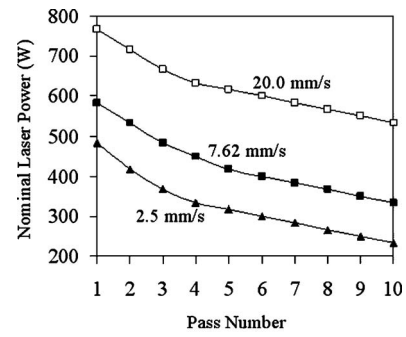


Fig. 5 Laser power used in the study. (a) Nominal laser power distribution at each pass for different laser travel velocities. (b) Laser power density along the travel direction from one side to another for each pass.

part receives an integrated heat which can affect the material properties including residual stress and mechanical strength due to tempering or aging effects [6].

The midpoints of layers 3, 5, and 10 have experienced similar thermal cycles as the midpoint of the first layer. The maximum temperatures of the midpoints in each layer are approximately the same. For the first five layers, the thermal cycles due to the reheat of subsequent passes will result in the transformation of tempered martensite. After the fifth layer is deposited, however, the temperatures at the upper part can never cool down to the martensite starting temperature. Therefore, for the upper part, martensite cannot be transformed during the deposition process, and fresh martensite will be transformed when the part is finished, which is consistent with the investigation of other researchers [2,12]. The possible tempered martensitic transformation of the lower layers will cause the hardness of the upper part to be higher than that of the lower part.

Figures 8–10 show the temperature distribution and phase proportions for each traverse speed at the time instant after the tenth layer is deposited. Higher traverse speed keeps the upper region of the part at higher temperature (Fig. 8(c)), which results in higher volume fraction of austenite (Fig. 9(c)) and lower volume fraction of martensite (Fig. 10(c)). The martensite present at lower layers is tempered martensite due to the thermal cycles. The austenite

Table 2 Processing parameters used in the study

Process parameters	Traverse speed (mm/s)	Moving time of the laser beam for each pass (s)	Idle time of consecutive layers deposition (s)	Time to finish one layer (s)	Total time to finish the part (s)
Case I	2.5	4	1	5	50
Case II	7.62	1.3	0.7	2	20
Case III	20.0	0.5	0.5	1	10

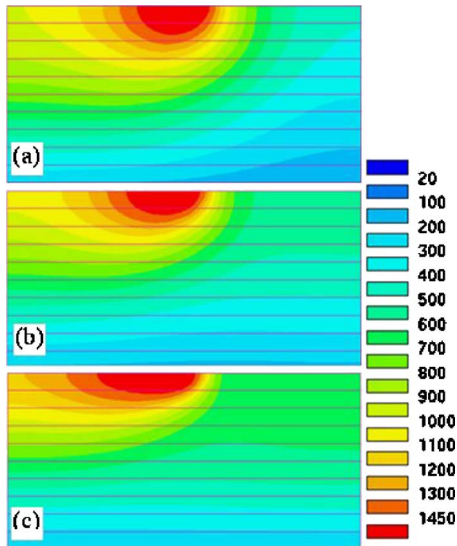


Fig. 6 Molten pool size and shape when the laser beam moves to the center of the part at the tenth layer for different traverse speeds. The molten pool size is determined by the melting temperature of SS410 (1450°C). (a) $V=2.5$ mm/s; (b) $V=7.62$ mm/s; and (c) $V=20$ mm/s.

present at the upper layers will be transformed to fresh martensite and retained austenite when the part cools down to the room temperature. This will result in higher hardness at the upper layers than at the lower layers. These simulations clearly indicate that higher traverse speeds produce more volume fraction of austenite, which transform to fresh martensite, resulting in more uniform microstructure and higher hardness.

An undesired defect that may occur in LENS-deposited parts is the presence of porosity. The pores can result from gas evolution during solidification or lack of fusion between layers of consecutive depositions surrounding the molten pool [5]. In the current study, a low volume fraction of austenite is observed at the beginning of each layer, in particular for high traverse speed (left side of Figs. 9(b) and 9(c)). The blue stripes in these figures actually are unmelted regions that did not receive enough power for the current traverse speed. This occurs at the beginning of the layer deposition because this region has had more time to cool before the deposition of the next layer starts. Similarly, the low volume fraction of martensite present at the lower layers (Fig. 10(c)) indicates the existence of unmelted powder due to the large heat dissipation of the substrate. Higher laser power is needed to fully melt the powder in the layers close to the substrate. These results provide some indications to illustrate the effect of the laser power and traverse speed on the porosity formation due to lack of fusion.

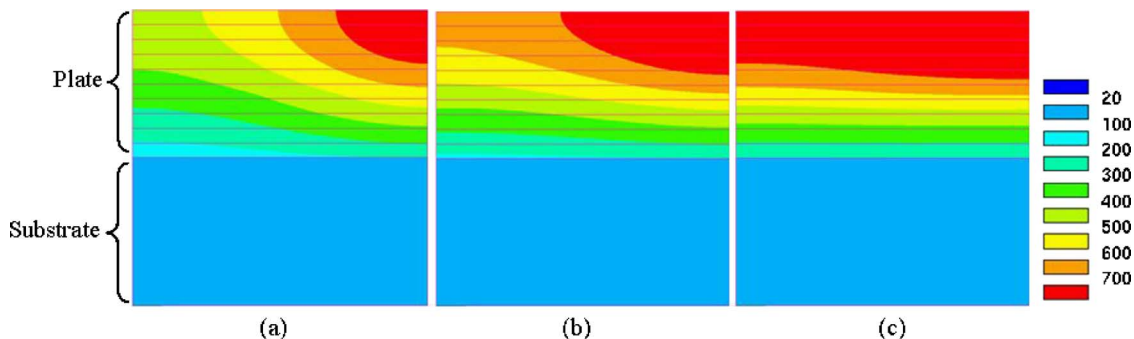


Fig. 8 Temperature field at the time instant after the tenth layer is deposited. (a) $V=2.5$ mm/s; (b) $V=7.62$ mm/s; and (c) $V=20$ mm/s.

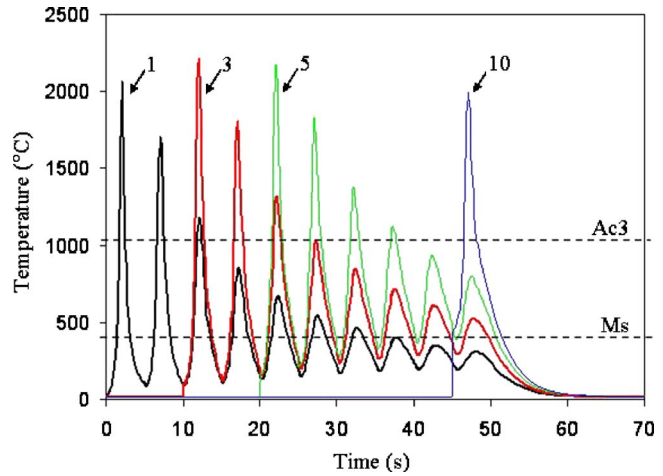


Fig. 7 Thermal cycles at the midpoints of layers 1, 3, 5, and 10 of the built part for laser speed $V=2.5$ mm/s

Figure 11 shows the temperature history at the center of the fourth layer for the laser speed of 2.5 mm/s. This location experiences seven thermal cycles before cooling down to room temperature. The location got a maximum temperature above the Ac_3 in the first four thermal cycles. Thus the calculation of phase proportions in the final state is started in the fifth thermal cycle. At the starting point of the fifth thermal cycle (point B shown in Fig. 11), the proportion of retained austenite is calculated by Eq. (4), where the temperature at point B is used, and equal to 305.3°C. Accordingly, the proportion of the retained austenite is equal to 61.2%. Similarly, the proportion of the retained austenite is calculated by Eq. (5) which yields 50.7% at point C and 1.3% at point D. In the final thermal cycle from point C to D, some retained austenite could transform to fresh martensite. The proportion of fresh martensite at point D is $50.7\% \times (1 - 0.013) = 50\%$. Thus the proportion of the tempered martensite at point D is $100\% - 50\% - 1.3\% = 48.7\%$. The final hardness at point D is 502.6 HV, calculated by Eq. (2).

Figure 12 shows the hardness distribution along the wall height center line for different laser speeds after the part cools down to room temperature. It is observed that the hardness is more uniform for higher laser speed than for the lower laser speeds. These results are qualitatively consistent with experimental data obtained by Griffith et al. [6]. They measured the hardness along the wall height center line of an H13 tool steel thin wall built by LENS deposition. Their data show higher hardness (59 HRC, 674 HV) in the upper region of the thin wall and lower hardness (45 HRC, 446 HV) at the bottom of the part.

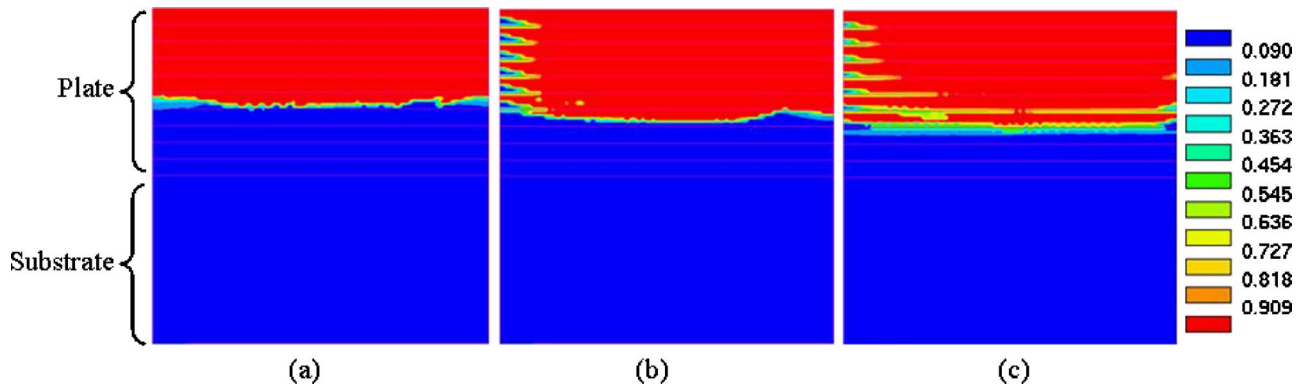


Fig. 9 Volume fraction of austenite at the time instant after the tenth layer is deposited. (a) $V=2.5$ mm/s; (b) $V=7.62$ mm/s; and (c) $V=20$ mm/s.

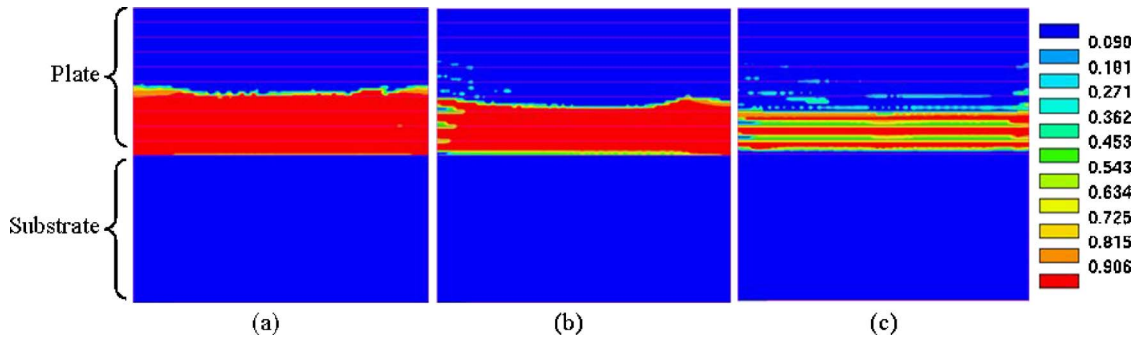


Fig. 10 Volume fraction of martensite at the time instant after the tenth layer is deposited. (a) $V=2.5$ mm/s; (b) $V=7.62$ mm/s; and (c) $V=20$ mm/s.

Summary of Original Contributions

Although higher travel speeds seem to be beneficial for the uniformity of the microstructure and hardness of the material, this can only be achieved with careful control of other process parameters. The main contribution of this work is to show the need to control laser power in order to obtain the desired results. This was not addressed in Costa et al. [12] and other modeling works [7] because the liquidus temperature of the alloy was used as bound-

ary condition in newly deposited elements, hence the effect of laser power is missed. Actually, measurements of the temperature in the molten pool have shown that the liquid is significantly superheated [3]. As illustrated in Fig. 5, the power must be adjusted not only from layer to layer, but also during deposition along a same layer in order to avoid edge effects. Insufficient laser power may result in porosity due to lack of fusion, while exces-

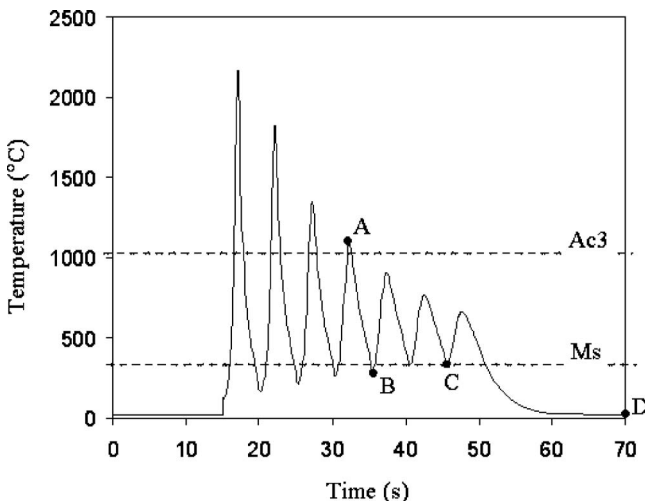


Fig. 11 Temperature distribution at the center of the fourth layer for $V=2.5$ mm/s

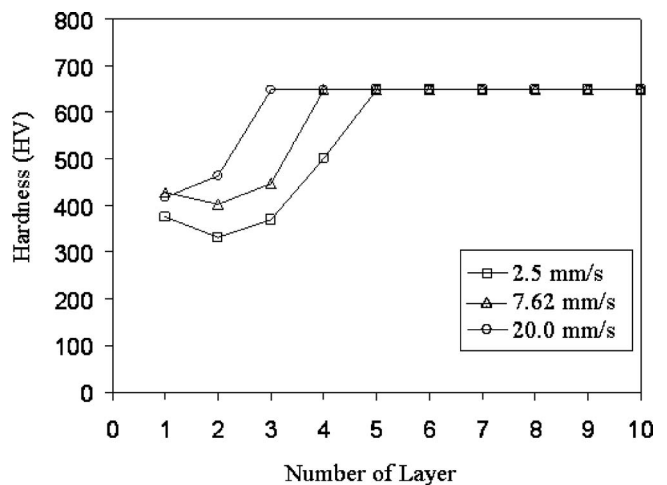


Fig. 12 Vickers hardness along the wall height center line for different laser speeds after the part cools down to room temperature

sive power may cause tempering of lower layers and consequent degradation of the material hardness and microstructure.

Conclusions

A three-dimensional finite element model has been developed and implemented to simulate the LENS deposition of a SS410 plate. The model was used to analyze the temperature distribution, molten pool size, and volume fraction of the solid phases formed at different traverse speeds. The laser power should be adjusted for each pass during the LENS deposition in order to keep a steady molten pool size. The modeling results show that a higher traverse speed can reduce the proportion of tempered martensite and achieve more uniform microstructure and hardness distribution in the plate. This is because a higher traverse speed allows most of the part to remain at temperatures higher than the martensite start temperature through the process, before it cools down to room temperature after the deposition is finished. However, higher traverse speeds can lead to the presence of porosity due to lack of fusion, particularly in the layers close to the substrate. Enough laser power is required for high traverse speeds in order to completely melt the powder and obtain a dense material.

Acknowledgment

The authors appreciate the sponsorship of the U.S. Army TACOM and the Center for Advanced Vehicular Systems (CAVS). We would like to thank Dr. John Berry of Mississippi State University, Jim Bullen of Optomec Co., and Benton Gady of National Automotive Center (NAC) for their helpful suggestions and guidance in this work. The support of Dr. Yogendra Gooroochurn (ESI) with SYSWELD is also appreciated.

References

- [1] Griffith, M. L., Ensz, M. T., Puskar, J. D., Robino, C. V., Brooks, J. A., Philliber, J. A., Smugeresky, J. E., and Hofmeister, W. H., 2000, "Understanding the Microstructure and Properties of Components Fabricated by Laser Engineered Net Shaping (LENS)," *Mater. Res. Soc. Symp. Proc.*, **625**, pp. 9–20.
- [2] Griffith, M. L., Schlienger, M. E., Harwell, L. D., Oliver, M. S., Baldwin, M. D., Ensz, M. T., Smugeresky, J. E., Essien, M., Brooks, J., Robino, C. V., Hofmeister, W. H., Wert, M. J., and Nelson, D. V., 1999, "Understanding Thermal Behavior in the LENS Process," *Mater. Des.*, **20**, pp. 107–114.
- [3] Hofmeister, W., Wert, M., Smugeresky, J., Philliber, J. A., Griffith, M., and Ensz, M., 1999, "Investigation of Solidification in the Laser Engineered Net Shaping (LENS) Process," *JOM*, **51**(7), *JOM-e* online www.tms.org/pubs/journals/JOM/9907/Hofmeister/Hofmeister-9907.html.
- [4] Atwood, C. L., Griffith, M. L., Schlienger, M. E., Harwell, L. D., Ensz, M. T., Keicher, D. M., Schlienger, M. E., Romero, J. A., and Smugeresky, J. E., 1998, "Laser Engineered Net Shaping (LENS): A Tool for Direct Fabrication of Metal Parts," *Proceedings of ICALEO*, Orlando, FL, pp. E-1.
- [5] Lewis, G. K., and Schlienger, E., 2000, "Practical Considerations and Capabilities for Laser Assisted Direct Metal Deposition," *Mater. Des.*, **21**, pp. 417–423.
- [6] Griffith, M. L., Schlienger, M. E., Harwell, L. D., Oliver, M. S., Baldwin, M.

- D., Ensz, M. T., Smugeresky, J. E., Essien, M., Brooks, J., Robino, C. V., Hofmeister, W. H., Wert, M. J., and Nelson, D. V., 1998, "Thermal Behavior in the LENS™ Process," *Proceedings of the Solid Freeform Fabrication Symposium*, Austin, TX, pp. 89–97.
- [7] Ye, R., Smugeresky, J. E., Zheng, B., Zhou, Y., and Lavernia, E. J., 2006, "Numerical Modeling of the Thermal Behavior during the LENS process," *Mater. Sci. Eng., A*, **428**, pp. 47–53.
- [8] Wang, L., and Felicelli, S. D., 2006, "Analysis of Thermal Phenomena in LENS™ Deposition," *Mater. Sci. Eng., A*, **435–436**, pp. 625–631.
- [9] Colaco, R., and Vilar, R., 2004, "Stabilization of Retained Austenite in Laser Surface Melted Tool Steels," *Mater. Sci. Eng., A*, **385**, pp. 123–127.
- [10] Colaco, R., and Vitar, R., 1998, "Effect of Laser Surface Melting on the Tempering Behavior of DIN X42Cr13 Stainless Tool Steel," *Scr. Mater.*, **38**, pp. 107–113.
- [11] Colaco, R., and Vitar, R., 1998, "Effect of the Processing Parameters on the Proportion of Retained Austenite in Laser Surface Melted Tool Steels," *J. Mater. Sci. Lett.*, **17**, pp. 563–567.
- [12] Costa, L., Vilar, R., Reti, T., and Deus, A. M., 2005, "Rapid Tooling by Laser Powder Deposition: Process Simulation Using Finite Element Analysis," *Acta Mater.*, **53**, pp. 3987–3999.
- [13] Costa, L., Elmer, J. W., and DebrRoy, T., 2002, "Simulation of Layer Overlap Tempering Kinetics in Steel Parts Deposited by Laser Cladding," *Proceedings of International Conference on Metal Powder Deposition for Rapid Manufacturing*, D. Keicher J. W. Sears, and J. E. Smugeresky, eds., MPIF, Princeton, NJ, pp. 172–176.
- [14] Costa, L., Vilar, R., Reti, T., Colaco, R., Deus, A. M., and Feide, I., 2005, "Simulation of Phase Transformations in Steel Parts Produced by Laser Powder Deposition," *Mater. Sci. Forum*, **473–474**, pp. 315–320.
- [15] Kelly, S. M., and Kampe, S. L., 2004, "Microstructural Evolution in Laser-Deposited Multilayer Ti-6Al-4V Builds: Part II. Thermal Modeling," *Metall. Mater. Trans. A*, **35**, pp. 1869–1879.
- [16] Labudovic, M., Hu, D., and Kovacevic, R., 2003, "A Three Dimensional Model for Direct Laser Metal Powder Deposition and Rapid Prototyping," *J. Mater. Sci.*, **38**, pp. 35–49.
- [17] Vasinonta, A., Beuth, J. L., and Griffith, M. L., "Process Maps for Controlling Residual Stress and Melt Pool Size in Laser-based SFF Processes," *Proceedings of the Solid Freeform Fabrication Symposium*, Austin, TX.
- [18] Wang, L., Felicelli, S. D., Gooroochurn, Y., Wang, P. T., and Horstemeyer, M. F., 2006, "Numerical Simulation of the Temperature Distribution and Solid-phase Evolution in the LENS™ Process," *Proceedings of the Seventeenth Solid Freeform Fabrication Symposium*, Austin, TX.
- [19] Toyserkani, E., Khajepour, A., and Corbin, S., 2004, "3-D Finite Element Modeling of Laser Cladding by Powder Injection: Effects of Laser Pulse Shaping on the Process," *Opt. Lasers Eng.*, **41**, pp. 849–867.
- [20] Ghosh, S., and Choi, J., 2006, "Modeling and Experimental Verification of Transient/Residual Stresses and Microstructure Formation of Multi-layer Aided DMD Process," *J. Heat Transfer*, **128**, pp. 662–679.
- [21] Qi, H., and Mazumder, J., 2006, "Numerical Simulation of Heat Transfer and Fluid Flow in Coaxial Laser Cladding Process for Direct Metal Deposition," *J. Appl. Phys.*, **100**, pp. 024903.
- [22] *SYSWELD 2005 Reference Manual*, ESI Group, Paris.
- [23] *SYSWELD 2005 Example Manual*, ESI Group, Paris.
- [24] *SYSTUS 2005 Analysis Reference Manual*, ESI Group, Paris.
- [25] Tsirkas, S. A., Papanikos, P., and Keramidis, Th., 2003, "Numerical Simulation of the Laser Welding Process in Butt-joint Specimens," *J. Mater. Process. Technol.*, **134**, pp. 59–69.
- [26] Unocic, R. R., and DuPont, J. N., 2004, "Process Efficiency Measurements in the Laser Engineered Net Shaping Process," *Metall. Mater. Trans. B*, **35**, pp. 143–152.
- [27] *ASM Handbook, Welding, Brazing, and Soldering*, 2005, ASM International, Material Park, OH, Vol. 6, pp. 438.